Journal of Power Sources 251 (2014) 243–253

Contents lists available at ScienceDirect

Journal of Power Sources

journal homepage: www.elsevier.com/locate/jpowsour

Methodology to optimize fluid-dynamic design in a redox cell

Juan Escudero-González, P. Amparo López-Jiménez*

Hydraulic and Environmental Engineering Department, Universitat Politècnica de València, Spain

HIGHLIGHTS

- Methodology proposed based on CFD, for optimizing redox cells design.
- Parameters definition: quantifying uniformity and symmetry of electrolyte velocity.
- Numerical techniques applied to velocity analysis (CFD and Hypothesis test).
- Case study using the methodology, defining an optimized redox cell geometry.

ARTICLE INFO

Article history:
Received 25 July 2013
Received in revised form
7 October 2013
Accepted 9 November 2013
Available online 3 December 2013

Keywords:
Redox cell
Computational fluid mechanics
Design optimization
Statistical analysis

ABSTRACT

The present work is aimed at the optimization of a redox cell design. The studied redox cell consists on a device designed to convert the energy of reactants into electrical energy when a liquid electrolyte reacts at the electrode in a conventional manner. In this particular sort of cells, the two electrolytes are present and separated by a proton exchange membrane. Therefore, the flow of the electrolyte and the interaction with the membrane takes a paramount importance for the general performance of the cell. A methodology for designing the inlet part of the cell based on optimizing the uniformity of the flow and the initial position of the membrane is presented in this study. This methodology, based on the definition and optimization of several parameters related to the electrolyte flow in different regions of the geometry, is depicted. The CFD (Computational Fluid Dynamics) model coupled with the statistical study pointed to several practical conclusions on how to improve the final geometry construction of the redox cell. A particular case study of redox cell is implemented in order to validate the proposed methodology.

1. Introduction

Redox Flow Cells are large stationary electricity storage systems. This sort of energy storage technologies will play a paramount role in the near future. The increasing use of efficient energy sources and renewable energy such as wind and solar, makes them necessary. These technologies usually suffer from experiencing intermittent generation [1] and the storage of energy is crucial to avoid the intermittency in the supply system.

The leading edge research impulses the development of energy storage to release the consumer system needs [2–4]. On a large scale, this energy storage could alleviate the unpredictability of energy sources to promote their accumulation over time [5].

Among these technologies, one of the most prominent is the redox flow battery (RFB). It is one of the best options for energy storage at medium and large scale [6]. The performance of these batteries is based on storing energy in solutions containing different redox couples. The electrodes surface makes possible the reversible electrodic processes. Redox and semi-redox technologies are good candidates for large stores of energy and medium domestic use storage, respectively [7].

On the one side, in this sort of batteries, the accumulated electrolyte determines the amount of energy stored. On the other side, the battery power depends on the electrode surface. The power stage is directly related to the active mass of the electrode, as the energy storage [8].

Accordingly, such batteries can modulate their output voltages and storage capabilities, and multiple cells can be interconnected using different sized reservoirs. Furthermore, they are very adequate as potential energy storage systems for distributed generation. In such cases the needs of each system determine their own requirements.

One of the first documented works on the redox flow cell was presented by Thaller in mid 1970s [9]. Since then, the redox flow cell concept has been implemented in different strategies, materials and chemical alternatives [10]. The numerically analysis of flow of electrolyte makes sense with the development of Computational Fluid Dynamics Technology (CFD), considering the precursors

* Corresponding author.
E-mail addresses: palopez@upv.es, palopezji@gmail.com (P.A. López-Jiménez).

0378-7753/$ – see front matter © 2013 Elsevier B.V. All rights reserved.
http://dx.doi.org/10.1016/j.jpowsour.2013.11.058

described in the papers of Frías-Ferrer [8] and Codina [11] Weber et al. 2011 [7] compile an interesting summary of Redox batteries. In these research conclusions it is highlighted that the future of this technology goes through optimizing designs modeling, both: flow and transport. In this sense, different materials have been applied in redox batteries, with different geometries [6,7,12].

Fig. 1 shows the scheduled diagram of a redox cell. The two cylinders placed on the sides of the figure represent the two electrolyte storage tanks. The tank on the negative electrode storages a redox solution, this solution will be different from the tank on the positive electrode. There are two pumps, one on each side of the reactor (Fig. 1). These pumps force the flow to circulate through the electrolyte in order to allow the semi-occurring redox reactions involving transfer of load.

The cathode is made of graphite of carbon felt. The anode is also made of graphite or carbon felt with a selective membrane as separator. The membranes are made up of cross-linked linear polymer chains, which form a three-dimensional network. Without the cross-linking, the membrane would be dissolved in water forming a polyelectrolyte solution. Ion exchange membranes have fixed ion functional groups and oppositely charged counter ions, present in sufficient numbers to render the whole exchanger electrically neutral. The reactions achieved in the cell (considered as an all-iron redox cell) are:

- $2Fe^{2+} \rightarrow 2Fe^{3+} + 2Fe$, during the charge
- $2Fe^{3+} + 2Fe \rightarrow 2Fe^{2+}$, during the discharge

The electrolyte composition for this purpose is 2 M $FeCl_2$ + 0.5 M NH_4Cl in deionized water, as based on [13]. The working temperature is 40 °C, the fluid viscosity at this temperature is $1.143 \cdot 10^{-3}$ (Ns m^{-2}). It has been assumed that the electrolytic fluid produces no deposition within the cell as well as it does not produce any gas phase. This hypothesis would be completely true if the redox reaction was 100% efficient. In reality, other competing reactions can occur with little gas production; these are disregarded as hypothesis [14]. Another assumed hypothesis is the one concerning the fluid density. Density is considered constant (1172 g m^{-3}) for all kind of flow.

The cell structure is surrounded by bipolar plates composed by structural support and electrical conductor. The electrodes, located on the side of each bipolar plate, are not involved in the electrochemical reactions. Nevertheless, they are important as they provide a surface facilitating the electron path. The membrane is located between both sides of the reactor. The membrane separates the two electrolytes, in order to preserve the electro-neutrality. The so considered volume 'A' (Fig. 1) is occupied by electrolyte. In this paper, the interest is focused on the uniformity of the electrolyte flow along this 'A' volume. Only the flow in the positive side of the cell is analyzed, as a symmetrical geometry is presented for both sides of the cell (positive and negative).

The uniformity of flow has a significant influence on the most important parameters of performance in the cell: the effective area of the electrode; the strength and efficiency; the useful life of the battery and electrochemical polarization (particularly under high current density variation [15]).

The consulted references propose that the flow of electrolyte through the active layer has a high inference performance thereof [16]. In 1998, Moyabayashi et al. [17] concluded that the increase in energy efficiency is essentially determined by a uniform distribution of electrolyte. However, although the flow is homogeneous, there could be significant local variations in the surface of the electrodes, among others, causing strong changes of pH. Furthermore, the interest between different geometries and flow conditions in different redox cells have been considered in the literature, focused on understanding and improving the functioning of the whole reactor [18–21] and the membrane position and configuration within the whole geometry [22].

Due to the fully compact battery system, the use of completely opaque key materials and the strong acidity of the electrolyte, the fluid distribution within the battery is often difficult to be determined, measured and quantified. However, the consulted references agree that research is vital to determine the optimal functioning of the battery pack [23,24].

Thus, the strategies for redox cell design should pay the most interest in the analysis of the velocities at all points of the trajectories of the fluid. It is especially interesting in the inlet part of the cell [25]. Nevertheless, an exhaustive treatment of these flow fields, especially in the design phase, requires two important numerical tools: on the one hand, Computational Fluid Dynamics (CFD) and on the other hand, statistical techniques. The use of CFD will help designers to simulate the velocity and pressure fields in the

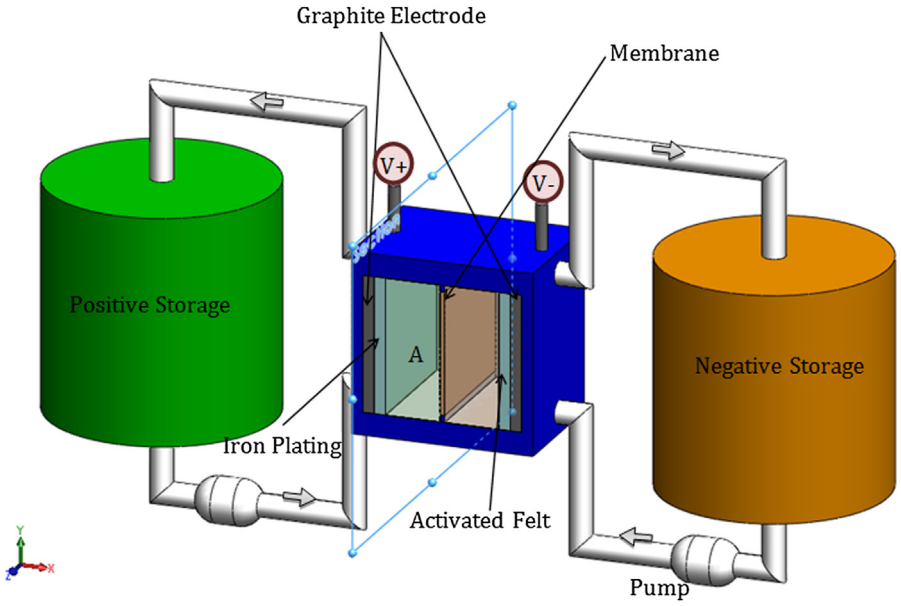

Fig. 1. Diagram of an iron flow battery (system components).

modeled geometry. This technique will suggest indicators of good performance of the design, allowing designers to compare different alternatives. Apart from this, statistical techniques will allow modelers to analyze the large number of individual generated velocities. The use of hypothesis test on these CFD data will help designers to analyze various aspects on the velocity fields. This will lead modelers to determine that some designs are better than others. Following the methodology here described, several statistical tests are proposed for the design of the distribution channels within a cell.

The purpose of this paper is therefore to propose and describe a methodology for analyzing the electrolyte flow rate of a Redox cell (Fig. 1). This methodology will reveal the uniformity in the velocity near the membrane, the most sensitive point for ionic interchange. With the use of the proposed performance indicators, the modeler will have tools for optimizing the design of the cell. Finally, an optimized geometry is proposed to be implemented in a real prototype.

2. The proposed methodology

The proposed methodology for designing redox cells considering flow uniformity is scheduled in Fig. 2. As it can be seen, this type of methodology has a well-defined and clear methodological approach.

The first step in this methodology is the definition of the initial geometry design. Afterward, three parameters are proposed to develop the cell geometry. They will be analyzed with the CFD and statistical tools (Fig. 2). Each parameter is focused on different parts of the geometry, as this methodology is a sequential analysis. The parameters are proposed to improve the cell geometry in order to ensure the flow uniformity near the membrane: Symmetry coefficient, Uniformity coefficient and Variability Range coefficient. These values will be further defined.

Some general initial boundary conditions used for this proposal methodology are:

- The range of flow rates for optimum operation is unknown. However, in this sort of cells, it is estimated that the value of the minimum flow is about 35 l h^{-1} (stoichiometric) and the maximum flow is around 150 l h^{-1}. The maximum flow is the most critical parameter that affects the design.
- The cell proposed is made up of 1 electron in the positive fluid and 2 electrons in the negative fluid.

Different efficient cell operation is caused by the velocity dispersion, for this reason it is important to analyze the velocity inside the cell, therefore the parameters to optimize and homogenize the inlet velocity and the inlet membrane velocity are proposed. The membrane is the most expensive part of this type of cell; it is around the 40% of the material cost [26]. The adequate behavior of the membrane depends on a correct interchange with the ionic flow. Furthermore, modeling the behavior of the flow in the cell is of paramount importance to ensure velocity uniformity [27] and then final performance in the cell.

The three parameters to be studied refer to different regions in the cell, described in Fig. 3, these parameters are: the Symmetry coefficient (evaluated in I region); the Uniformity coefficient (assessed in the E region); and Variability Range coefficient (considered in the M region).

- I region: This part refers to the entrance of the cell. In this region the symmetric flow is analyzed. The Symmetry coefficient (C_U) will be defined to quantify the performance in this region.
- E region: This zone refers to the exit at the end of the channels. The parameter used to analyze this region is the Uniformity coefficient (C_H) and it defines the average velocity per channels.
- M region: This one refers to the region located after the channels at the same distance of the membrane location. The Variability Range coefficient of velocity front (R_I) and maximum and minimum value of velocity is defined with the purpose of selecting the best position of the membrane.

As it has been mentioned, the numerical tools used for this methodology are the Computational Fluid Dynamics and the Hypothesis test, which will be simply described.

2.1. CFD analyses of the velocity field

A general purpose computational fluid dynamic software package has been employed to run the simulations: Star CCM+. The computational model solves numerically the governing laws of Fluid Dynamics. These equations, taking into account turbulent phenomena, are solved in a geometrical domain, given a number of

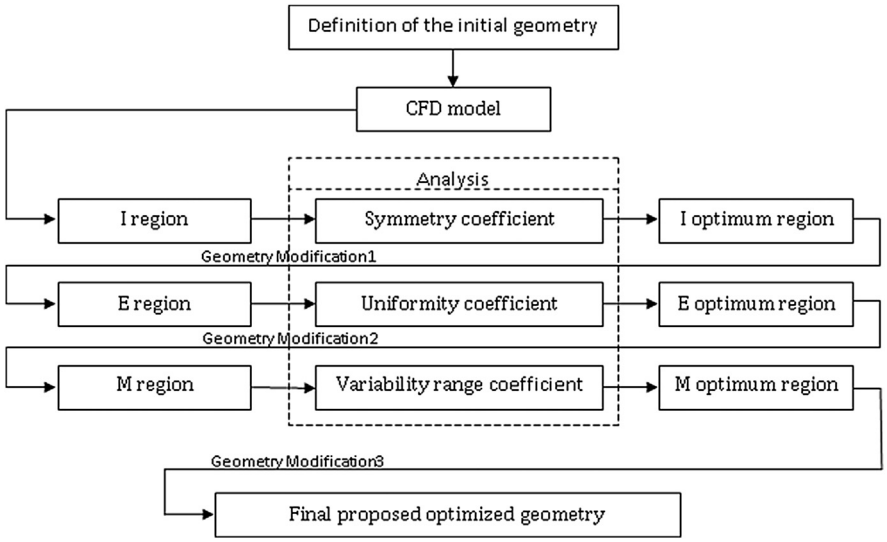

Fig. 2. Diagram of proposed methodology.

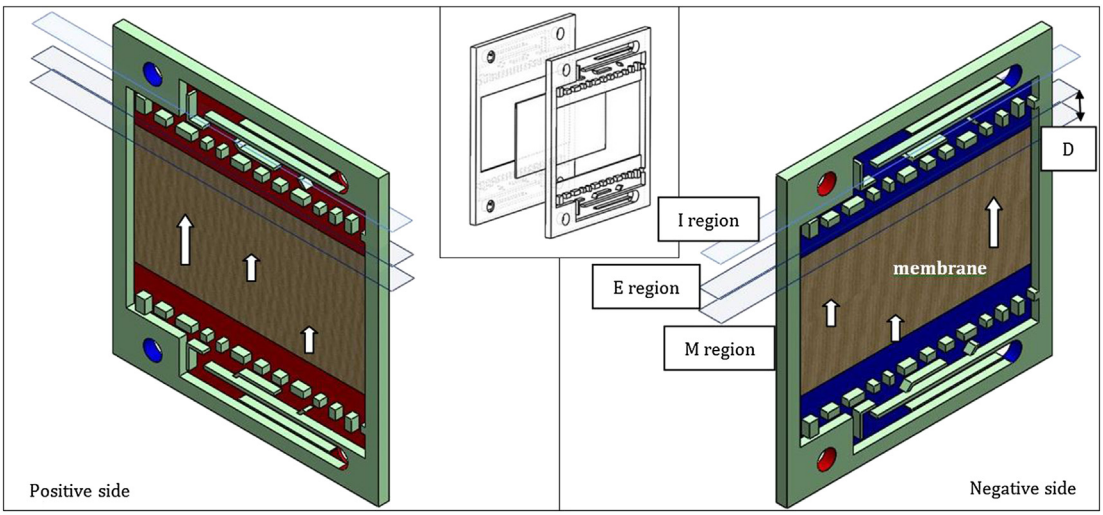

Fig. 3. Commercial cell geometry.

suitable boundary conditions. In a CFD the relevant magnitudes (velocity) are calculated in a discrete manner at the nodes of a certain mesh or grid and they are represented along the mesh. The use of these computational tools to gain insight into the velocity field of the modeled flows currently constitutes a powerful tool for designers in devices involving fluid motion.

The advantage of using these models is that they can simulate real problems of Fluid Mechanics to any degree of complexity. Furthermore, they can help modelers to visualize hydrodynamic aspects otherwise impossible to be measured or represented in a real case (i.e. stream lines) that have great importance in the comprehension of the studied phenomena. The conservation equations solved by the code are those of mass and momentum. The continuity or mass conservation equation solved is the expression (1).

$$\frac{\partial \rho}{\partial t} + \nabla \rho \vec{v} = S_{\mathrm{m}} \tag{1}$$

where ρ is the fluid density, $\vec{v}$ is velocity and S_{m} represents the mass source contained in the control volume. For other geometries, suitable coordinates, namely spherical or cylindrical, should be used. Also, the momentum equation is considered by the equation (2).

$$\frac{\partial (\rho \vec{v})}{\partial t} + \nabla \rho (\vec{v}\vec{v}) = -\nabla p + \nabla \tau + \rho g + F \tag{2}$$

where p is the static pressure; the gravitational and outer forces defined on the control volume respectively, and $\bar{\tau}$ the stress tensor, expression (3), where μ is the eddy viscosity. I is the unit tensor and the third term accounts for the effect of the expansion of volume.

$$\tau = \mu \left[\left(\nabla \vec{v} + \nabla \vec{v}^{T} \right) - \frac{2}{3} \nabla \vec{v} I \right] \tag{3}$$

All conditions and properties are defined via STAR-CCM+ and solved using the coupled solver. The results are displayed via post-processing tools available. The volume mesh in a simulation is the mathematical description of the space (or geometry) of the problem being solved. The geometry model is designed to work on three-dimensional meshes.

Before introducing the geometry in the calculation software, the geometry must be properly prepared. To do this, the geometry of the experiment has been modeled using commercial CAD software. Once the geometry of the reactor is represented, it is imported to the calculation software and the meshing process is performed on the fluid domain.

The trimmed mesh has been chosen due to the flow movement by using the trimmer wake refinement and the volume shape tools in areas where a fine mesh is needed. Optimized mesh main parameters are described in Table 1.

The here proposed methodology is aimed to compare different geometrical alternatives for the cell under the same initial flow conditions. In this sense all the quantifications are based on CFD techniques. The particular numerical model implemented does not consider deformable meshes for calculations. However, in the real world, redox-flow battery stacks are not completely rigid, therefore, the distribution in the porous electrodes is subjected to change once the membrane or the bipolar plates are deformed by flow/pressure distribution. These changes in the mesh have not been considered in this model. This is a potential limitation for the validity of the numerical model.

An input speed and an output pressure of the model have been designed. The other boundaries are represented by a wall condition; the one used by the computational code is similar to the one called 'smooth tube roughness' [28] that is well suited to the material properties of the cell.

The selective membrane does not affect the hydrodynamic movement of the fluid, as there is no pass of fluid across the membrane; only electronic transfer occurs in this process. As this does not affect velocity, pressure or turbulence, the boundary condition implemented for the membrane is wall.

Once the boundary conditions have been well-defined and a suitable mesh in the full model is implemented, the computer code solves the equations of movement (conservation of mass or

Table 1
Optimized mesh features.

Base size (mm)	3	Surface curvature (pts./circle)	72
Relative minimum size (mm)	1.5	Maximum cell size (mm)	6
Relative target size (mm)	3	Remeshed surface (FACES)	491, 314
Volume mesh (final proposed optimized geometry)	655, 913		

continuity (4), and conservation of movement quantity or Navier–Stokes (5)).

$$\nabla \overline{U} = 0 \tag{4}$$

$$\frac{\partial \overline{U}}{\partial t} + \nabla(\overline{UU}) - \nabla(\nu \nabla \overline{U}) = -\nabla \overline{p} + \overline{U\prime U\prime} \tag{5}$$

where U represents the velocity vector, U′ indicates fluctuations around the value of the mean velocity, p is the dynamic pressure, ν is the kinematic viscosity and $\overline{U\prime U\prime}$ represents the so-called Reynolds stresses. In laminar flow conditions, the average velocities coincide with the snapshots and the Reynolds term vanishes, leading to a closed system of equations, which requires no turbulent solutions. In turbulent flow, as Reynolds stresses are not canceled, close solutions are needed which provide the sufficient equations to know the instantaneous velocities throughout the domain. At low Reynolds numbers, the most indicated solutions are k-Epsilon [29–31]. The Bibliography is profuse in the use of these techniques in similar engineering problems [32,33] even in modeling environments close to the here described technique [34,35].

In this modeling, three-dimensional simulations were performed using the STAR-CCM+ software. This is based on the finite volume method (FVM) to solve the conservation of mass equation and the Navier–Stokes averaged equations in a curvilinear mesh, not taking into account the effects of temperature. Second order upwind scheme is used in this case for discretization. The advantage of this scheme over the first-order upwind scheme is that it is nominally second-order accurate. In order to meet the mass conservation condition a correction algorithm standard pressure (SIMPLE) is used. Thus, the code solves algebraic and iteratively equations considering gravity at all times until the residue numbers values are sufficiently low (less than 10^{-3}) considering that the resolution has converged.

2.2. Hypothesis testing applied on the CFD data

The goal in Hypothesis Testing [36,37] is to analyze a sample of data in an attempt to distinguish between population characteristics that are likely to occur and population characteristics that are unlikely to occur.

There are two main keys in hypothesis testing such as null hypothesis and alternative hypothesis. On one hand, null hypothesis is a statement about the value of a population parameter (in our case *mean channel speed MCS*), represented by H_0 and always stated, in statistical terms, as an equality (=). On the other hand, alternative hypothesis is a statement about the value of a population parameter that must be true if the null hypothesis is false and is represented by H_1 and stated as an inequality (<,>,≠). Then formulated both, null and alternative hypothesis, in terms of the model parameter MCS.

$$H_0: \text{MCS are the same in two different channels} \rightarrow \mu_i = \mu_j \forall\ i \neq j \tag{6}$$

$$H_1: \text{MCS are NOT the same in two different channels} \rightarrow \mu_i \neq \mu_j \forall\ i \neq j \tag{7}$$

Our model has a total of 84 channels to be analyzed.

Any variation detected with a p-value ≤0.05 (this value is the level of significance of the test denoted using Greek letter α) is due to random phenomena intrinsic to the system, also called natural process variability.

Samples of all channels are obtained together for a particular run of Computational Fluid Dynamics scenario, since it is a stochastic process. The distribution of the average speed on all channels is known:

$$\overline{x}_{\text{channel\_}i} \approx N\left(\mu_i, \frac{\sigma_i}{\sqrt{n_i}}\right) \tag{8}$$

$$\overline{x}_{\text{channel\_}j} \approx N\left(\mu_j, \frac{\sigma_j}{\sqrt{n_j}}\right) \tag{9}$$

Every probability density function of speed is dependent from the point of view of the channels' distribution. The statistic used is the difference of sample means which is the non-centered moment of order {r ∈ N|r: 1} and since the difference of two normal distributions is a normal distribution yet, this gives:

$$\overline{x}_i - \overline{x}_j \approx N\left(\mu_i - \mu_j, \sqrt{\sigma_i^2 + \sigma_j^2 - 2Cov(x_i, x_j)}\right) \tag{10}$$

To use the normal distribution, values of simple data are first converted to standardized Z scores using the following transformation:

$$Z = \frac{(\overline{x}_i - \overline{x}_j) - \left(\mu_i - \mu_j\right)}{\sqrt{\sigma_i^2 + \sigma_j^2 - 2Cov(x_i, x_j)}} \approx N(0,1) \tag{11}$$

Z scores transforms data into the standard cumulative normal distribution whose mean is 0, and variance is 1. Z-scores provide a mapping from a distribution of some variable to a standardized scale. These mappings reflect the difference in terms of number of standard deviations away from the mean.

Because of the size of sample data is greater than 30, this is the reason we choose Z-scores as statistic parameter instead of t-Student.

Equations (12) and (13) summarize the main ideas in hypothesis testing:

$$\text{Fail rejection region}: \left\{ -z_{(\alpha/2)} \leq Z \leq z_{(\alpha/2)} \right\} \tag{12}$$

$$\text{Rejection region}: \{Z \in \text{to any other region}\} \tag{13}$$

Once exposed to perform hypothesis testing, this has to be applied. The mean speed at every channel is represented by a histogram; therefore, this plot represents the difference among channels, and with a simple glance detects which MCS are quite different among themselves.

By examining the results of hypothesis testing applied to the sample, the null hypothesis can be rejected or failed to be rejected. It will indicate which channels are significantly different from each other. In order to not introduce error analysis, the comparison made by hypothesis testing is performed 1-by 1 channel. The total numbers of comparisons are $\sum_{i=1}^{\text{Total\_channels}-1} i = 3486$. Doing 1-by-1 comparisons among the total number of channels, errors are avoided.

3. Proposed parameters analysis

The here depicted methodology is based on three different parameters to be considered: the Symmetry coefficient, Uniformity coefficient and Variability Range coefficient of velocity front.

3.1. Symmetry coefficient

The Symmetry coefficient is the first parameter to be analyzed; it indicates the amount and the longitudinal distribution of flow

that goes inside the cell. A poor distribution of the flow affects noticeably the correct distribution of the fluid.

To evaluate this coefficient it is necessary to know about the flow circulation along the cell. The coefficients (C_{S_A}, C_{S_B}) evaluate the percentage of flow on left and right side of the cell. This parameter is analyzed in I region.

$$C_{S\_A} = \frac{Q_i}{Q_T} = \frac{\sum_{i=0}^{n/2} v_i S_i}{\sum_{i=0}^{n} v_i S_i} \tag{14}$$

$$C_{S\_B} = \frac{Q_i}{Q_T} = \frac{\sum_{i=n/2}^{n} v_i S_i}{\sum_{i=0}^{n} v_i S_i} \tag{15}$$

- $v_i = i$ velocity channel.
- $S_i = i$ area channel.

The best design will be the one that shows coefficient (C_{S_A}) to be similar to coefficient (C_{S_B}); this design distributes the flow uniformity around the cell. To evaluate the optimum design the Symmetry coefficient is proposed. The best design will be the one presenting a minimum coefficient. This Symmetry coefficient is defined by (16):

$$C_U = \frac{C_{S\_A} - C_{S\_B}}{C_{S\_A}} \tag{16}$$

3.2. Uniformity coefficient

This coefficient evaluates the velocity for each channel, in this particular case, the goal is to maintain a constant velocity inside the cell and this can be analyzed with the uniformity statistic coefficient. This means that a lower Uniformity coefficient represents similar velocities of the channel output and this would be a good design.

The null hypothesis is true when the velocity of one channel is equal to the other channel and the alternative hypothesis occurs when the velocities are different. Therefore, the Uniformity coefficient is defined, in this case, as the relation between the null and the alternative hypothesis.

$$C_H = \frac{\sum\left(-z_{\alpha/2} \le Z \le z_{\alpha/2}\right)}{\sum(Z)} \tag{17}$$

A good design is supposed when the Uniformity coefficient is lower. Nevertheless, it is true that it could be represented by a punctual error because the design could have a very high coefficient through few channels. For this reason, it is very important to design a frequency graph to represent the accumulated errors in two dimensions (E region, Fig. 3).

With the implementation of this parameter it is possible to only focus the cell design in the errors channels and improve it step by step.

3.3. Variability Range coefficient of velocity front

The Uniformity coefficient is obtained by the hypothesis test, if this coefficient is small; the velocity inside the channels presents more uniformity. Nevertheless, it does not solve all problems that are present in the design and for this reason it is necessary to define another parameter: the Variability Range coefficient of velocity front. It is evaluated in a range of D distances of the membrane (M region, Fig. 3).

This analysis allows modelers to determine the variability range of front velocity (maximum velocity and minimum velocity) and the interpolation curve. The position of the membrane will be determined by the correct processing of these data fields.

First of all, it is necessary to obtain the velocity data with the CFD tools. Then, these data are treated mathematically and cleaned if it is necessary. The obtained range is the difference between maximum and minimum velocity value. The aim of this point is to achieve the lowest range value.

Interpolation polynomial must be applied for the mathematical analysis, because it is a good tool to determinate the area that has a higher speed or slower than the medium velocity. The interpolator polynomial moves until the velocity average is situated in the coordinate's axis. Furthermore it is possible to calculate the above and underneath region by means of integration in the interpolator polynomial. In this case, the area is positive when the velocity is higher than the medium velocity and the area is negative when the velocity is lower than the medium velocity.

$$U = |U_+ - U_-| \tag{18}$$

It is necessary to define two criteria to evaluate this coefficient; equations (19) and (20); the correct location of the membrane is determined for the range and the interpolated area, so, it is necessary to minimize the range and the interpolated area.

$$R_i = V_{\max,f} - V_{\min,f} \tag{19}$$

$$R_i < V_{m,t} \tag{20}$$

4. Case study: particular design of a redox cell

In order to apply the methodology described here, a particular design is proposed. The objective is to obtain the geometry in which the flow is as much uniform as possible, considering the modification of several geometrical aspects.

4.1. Symmetry coefficient. Geometry modification 1

Symmetry coefficient is affected by the displacement of the cell inlet geometry radius. Therefore displacement (D_1) and (D_2) affects both radius positions (Fig. 4). As these radiuses directly concern the symmetry flow, the displacement of the radius was decided. If this parameter is amended, the asymmetry will be compensated because the inlet and the outlet are only in one side of the cell. Fig. 4 and Table 2 represent the considered changes in the D_1 and the D_2.

In the bar diagram depicted in Fig. 5, the Symmetry coefficient, C_U evaluated by expression (16), can be seen.

Fig. 4 and Table 2 depict the little changes proposed in the inlet region in order to improve the symmetry of the velocity fields in I region. It's evaluated with the Symmetry coefficient, further quantified in Fig. 5. In order to provide more information about how these changes affect the velocity profiles, Fig. 6 is presented. In this Figure, the velocity magnitude for the nodes located along I region is represented in modulus, versus position for a) and c) alternatives. As it can be seen, the velocity profile resulting in c) alternative is more symmetrical. Left side velocity profile in a) alternative achieves considerably smaller values than right side velocity profiles. As the difference between these both velocities profiles affect the Symmetry coefficient, the c) alternative present's smaller coefficient and therefore better symmetry.

The optimum velocity in I region is the c) alternative, where the value of the Symmetry coefficient is 2.39%; this means that only a

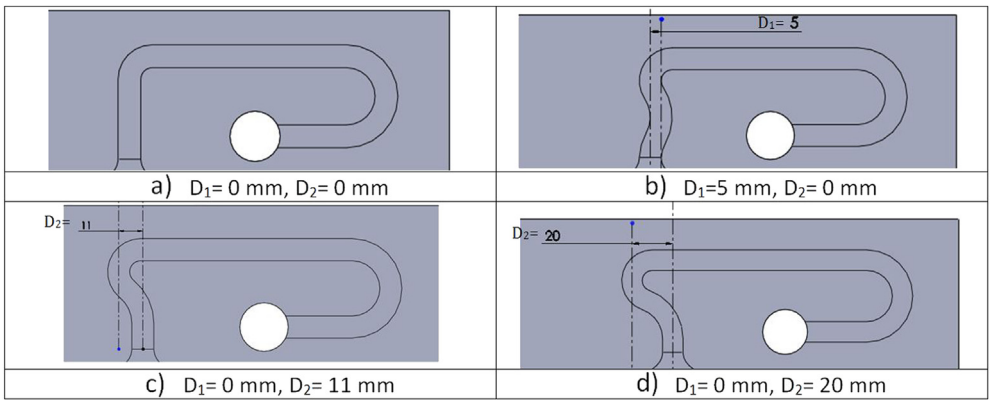

Fig. 4. Symmetry alternatives of design.

Table 2
Alternatives for radius of design.

	a) alternative	b) alternative	c) alternative	d) alternative
D_1 (mm)	0	5	0	0
D_2 (mm)	0	0	11	20

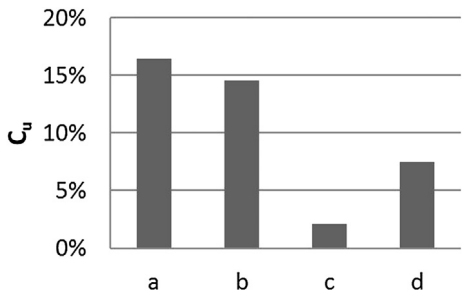

Fig. 5. Symmetry coefficient evaluated.

2.39% of the flow is asymmetric for a specific flow of 150 l h^{-1}. The optimum region features are:

- D_1: 0 mm.
- D_2: 11 mm.

4.2. Uniformity coefficient. Geometry modification 2

The Uniformity coefficient is obtained, considered in the E region (Fig. 3). The hypothesis test is used as it has been described in Section 2.2. If the velocity of channel 1 is statistically significant to the one in the other channel, the null hypothesis is true; in this case, it is evaluated $\sum_{i=1}^{83} i = 3486$ cases.

The Uniformity coefficient is defined as the relation between the null hypothesis and all of these cases (equation (17)). With this specific coefficient we can obtain a numerical comparison among different geometries.

The changes in the geometry affect inside the cell, in the E region. This area has been changed to obtain the lowest value of the uniformity coefficient. Fig. 7 shows the four different geometries analyzed with same flow. To do so, c) alternative of Fig. 4 is represented in these possibilities.

Once the geometry changes have occurred, the Uniformity coefficient (C_H) for the e), f), g) and h) alternatives are represented in Fig. 8. In the bar diagram, the changes on the geometry influence can be seen. The lowest coefficient is the g) alternative, with a value of a 4.8% of uniformity. It means that only 4.8% of channels have a different value for mean velocity.

As it can be seen in Fig. 9, the modulus of velocities in the nodes located in E region show less variation in g) alternative than those

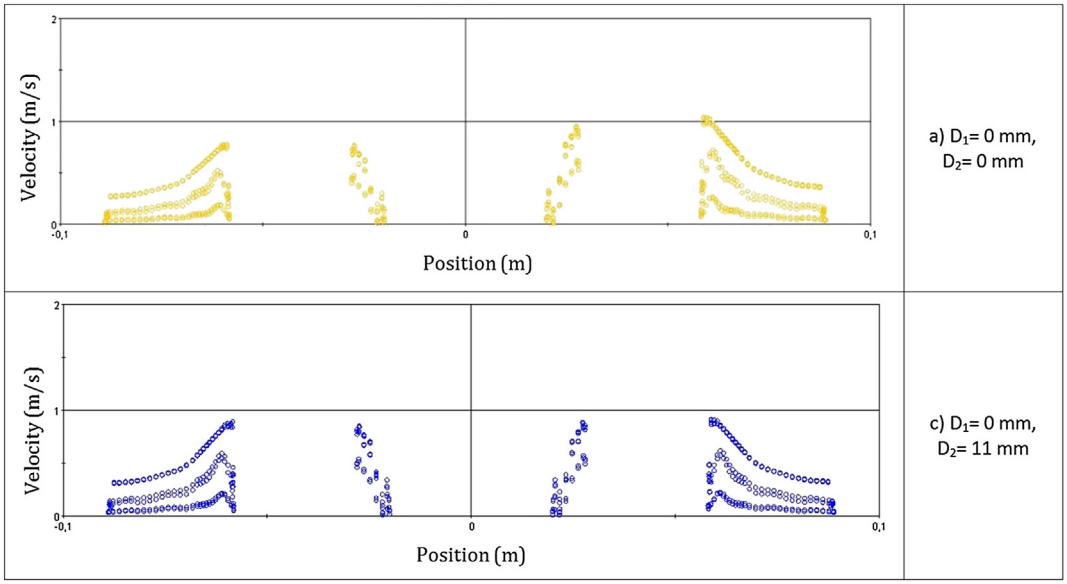

Fig. 6. Velocity profiles: a) and c) alternative.

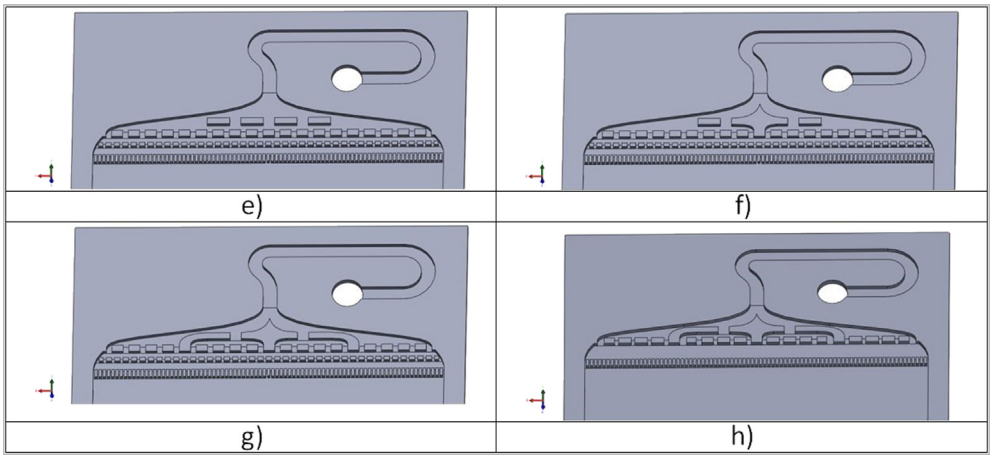

Fig. 7. Uniformity alternatives of design.

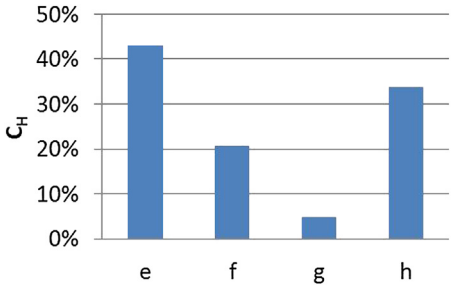

Fig. 8. Uniformity coefficient evaluated.

in e) alternative. The velocities are, therefore, more uniform along E region and the range of variation is smaller in g) alternative.

A visual study is necessary to validate the symmetry and Uniformity coefficient previously described. For this reason, a frequency graph (Fig. 10) is used to validate the technique mentioned and to represent the velocity differences in every channel. This diagram is a powerful tool to analyze velocities inside the cell because you can identify which channels are problematic.

The *x*-axis determines the number of channels (84) and the *y*-axis determines the channels rejecting the null hypothesis (83 possibilities). If the C_H coefficient is small, the average velocities of the channels are more equal and are represented by an empty bar diagram.

For the optimum geometry (g) alternative) design, channels with different velocities are represented in Fig. 10 Additionally, the Symmetry coefficient can also be seen in the bar graph. A velocity symmetrical distribution is observed.

4.3. Variability Range coefficient of velocity front. Geometry modification 3

Finally, Variability Range coefficient is analyzed; this coefficient determines the position of the membrane. In order to experience a good functioning of the membrane, the velocity should be constant at the beginning of the membrane. The velocity at the position of the membrane is analyzed in this point. To do so, the 19 equation (distance *D*, Fig. 3) is proposed.

The variability coefficient of the range is represented in Fig. 11. This range decreases as the membrane distance (*D*) increases.

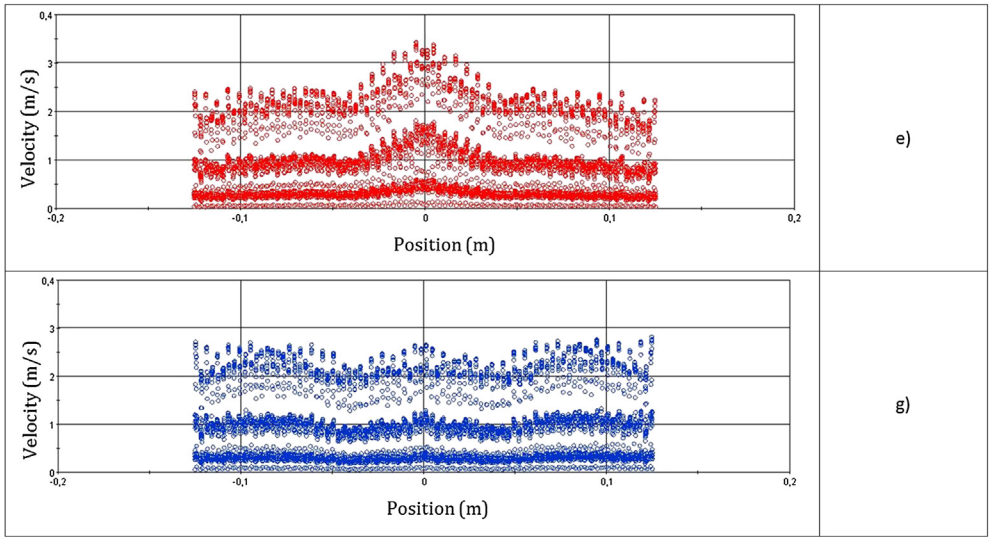

Fig. 9. Velocity profiles, e) and g) alternative.

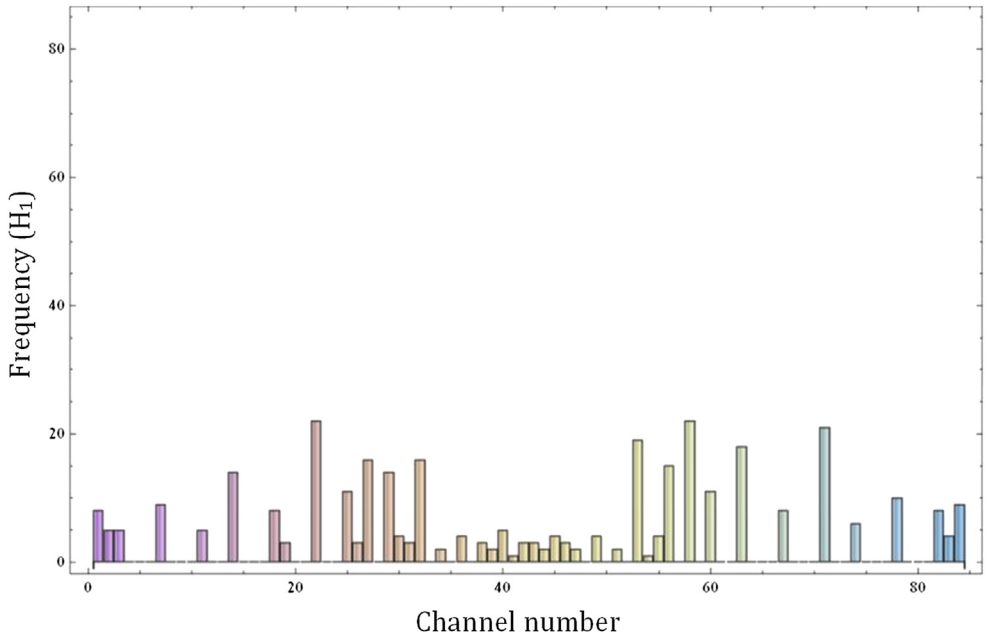

Fig. 10. Bar graph of g) alternative.

Therefore, the evolution of the range coefficient of velocity front is decreasing in this case.

Furthermore, another aspect is also analyzed around the variability range. An Interpolator polynomial is used to model the curve of the velocity front with the intention of obtaining the area (equation (18)) above or below the medium velocity. Fig. 12 shows the evolution of this area in four different points. As represented in the figure, when increasing the distance (D) the net area above or below the medium velocity decreases; in addition, the membrane inlet velocity is more uniform.

The theoretical average velocity is 0.52 m s^{-1} based on the analysis of Figs. 11 and 12, and the criterion set out in equation (20), the optimum distance is 30 mm. This is a design criterion and for other applications of this methodology, it could vary depending of the designer.

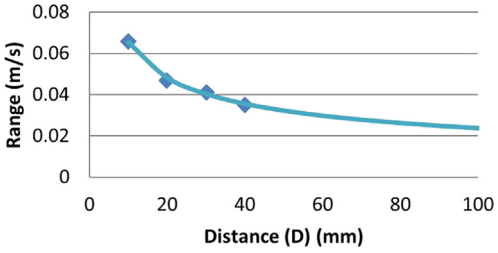

Fig. 11. Velocity range.

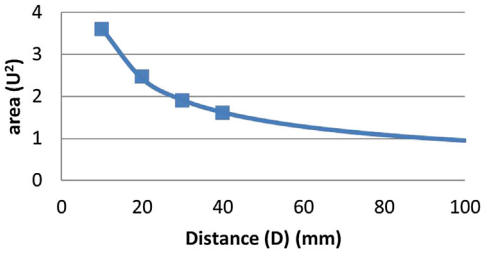

Fig. 12. Interpolator polynomial area.

The Interpolator polynomial, maximum and minimum velocity for the distance suggested of 30 mm is represented in Fig. 13.

4.4. Final proposed model

From the analysis of all coefficient and geometry described in the preceding epigraphs, an optimum geometry of a full cell is

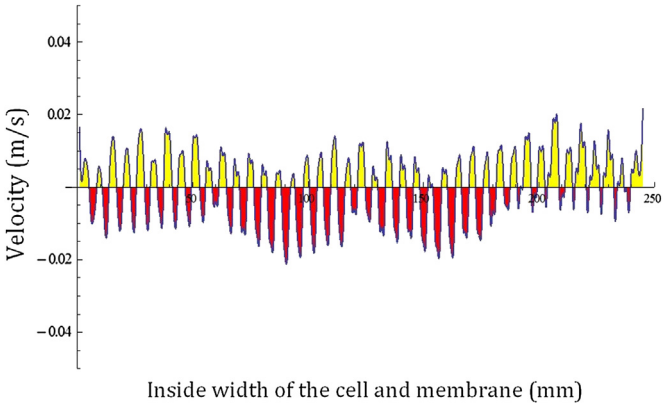

Fig. 13. Interpolation polynomial, $D = 30$ mm.

Fig. 14. Final optimized geometry.

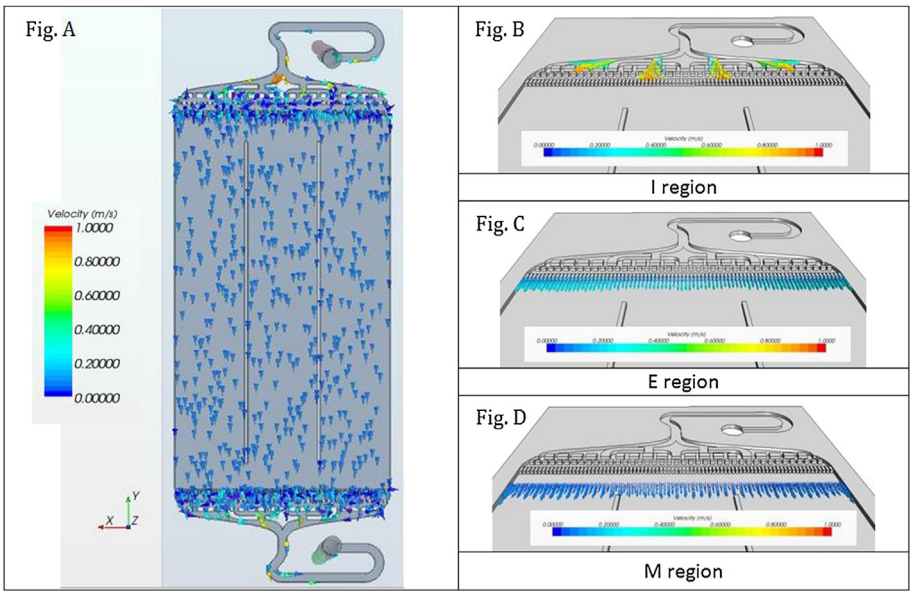

Fig. 15. Velocity vectors of the final geometry, I region, E region and M region.

proposed. In this improved geometry, the velocity is more symmetric and uniform than in the initial geometry; therefore the ionic exchange will be produced in all the membrane, as dead zones (regions will null velocity) will not appear.

Fig. 14 shows the final optimized geometry for the whole cell. The two rib lines are included in the design to achieve higher structural resistance. This is a step further to ensure the cell rigidity and to maintain the distance between the membrane and the electrode. These ribs will not affect the velocity field in the studied design regions.

In this case, some CFD representations of velocity vectors are provided in Fig. 15. The velocity vectors along the proposed geometry are shown (Fig. 15a). The initial flow distribution in both sides of the geometry is observed in I region, with a great symmetrical behavior (Fig. 15b). When the flow has passed across all the channels, the most uniform velocity vectors profile is observed in E region (Fig. 15c). Finally, as expected, when the flow overcomes the membrane in M region the velocity is symmetrical, uniform and with a small variability, as expected (Fig. 15d).

In future researches, this geometry will be build and the velocity profile will be visualized to validate the here proposed methodology.

5. Conclusions

In this contribution, a methodology has been presented to help modelers to take decisions about the fluid-dynamic design in a redox cell. The methodology is based on the definition of three performance indicators: the Symmetry coefficient, Uniformity coefficient and Variability Range coefficient. These parameters will help to quantify the flow uniformity of the cell final design.

The Symmetry coefficient indicates the amount and the longitudinal distribution of flow that goes inside the cell. In order to get these velocity profiles, a deep CFD analysis has been implemented.

The Uniformity coefficient evaluates the velocity for each channel. In this particular case; the aim is to maintain a constant velocity inside the cell. In order to get this coefficient, a Hypothesis test technique has been proposed, based on the CFD results, to check if the velocity profiles from different channels are equals or not.

Finally, a Variability Range coefficient is proposed. The velocity at a specific point of the membrane is analyzed to determine the velocity front variability. The objective is to find the more convenient position for the membrane with a constant velocity profile, as near as possible from the geometry channels.

The sequential consideration of these three parameters will let the modeler to determine the number of inlet channels, the distance among them and the configuration of the inlet geometry in order to make the velocity uniform when the fluid touches the membrane.

A case study is presented to illustrate the capability of the depicted methodology. An optimum geometry is generated for a 150 l h^{-1} cell. In this case, the proposed parameters have been used to determine the most convenient geometry among many different alternatives. A final design, in which only 4.8% of the channels have a different value for mean velocity, has been proposed. This is a very uniform velocity for the flow arriving to the membrane.

In future research, this real cell geometry is going to be built in order to validate the velocity distribution provided by the CFD and the here proposed methodology. Further CFD models will have to consider the interaction between fluid and the solid boundaries. The influence of cell rigidity on the performance of the overall cell will be also analyzed in future studies.

References

[1] M. Skyllas-Kazacos, M.H. Chakrabarti, S.A. Hajimolana, F.S. Mjalli, M. Saleem, J. Electrochem. Soc. 158 (2011) 55–79.
[2] M. Rychcik, M. Skyllas-Kazacos, J. Power Sources 22 (1987) 59–67.
[3] R.M. Dell, D.A.J. Rand, J. Power Sources 100 (2001) 2–17.
[4] Z. Yang, J. Zhang, M.C.W. Kintner-Meyer, X. Lu, D. Choi, J.P. Lemmon, J. Liu, Chem. Rev. 111 (2011) 3577–3613.
[5] L. Joerissen, J. Garche, C. Fabjan, G. Tomazic, J. Power Sources 127 (2004) 98–104.
[6] C. Ponce de Leon, A. Frias-Ferrer, J. Gonzalez-Garcıa, D.A. Szanto, F.C. Walsh, J. Power Sources 160 (2006) 716–732.
[7] A. Weber, M. Mench, J. Meyers, P. Ross, J. Gostick, Q. Liu, J. Appl. Electrochem. 41 (2011) 1137–1164.
[8] A.J. Frías-Ferrer, Optimización de la hidrodinámica de reactores electroquímicos: empleo de métodos experimentales y numéricos, Tesis doctoral, Universidad de Alicante, Spain, 2004.
[9] L.H. Thaller, in: Proceedings of the 9th Intersociety Energy Conversion Engineering Conference, San Francisco, California, USA, 1974.
[10] A. Parasuramana, T.A. Lima, C. Menictas, M. Skyllas-Kazacos, Electrochim. Acta 101 (2012) 27–40.
[11] G. Codina, Desarrollo de una planta de acumulación de energía eléctrica basada en el acumulador redox Fe/Cr, Tesis Doctoral, Universidad de Alicante, Spain, 1992.

[12] S. Eckroad, Vanadium Redox Flow Batteries: an In-depth Analysis, EPRI, Palo Alto, CA, 2007.
[13] J. Mellentine, Performance Characterization and Cost Assessment of an Iron Hybrid Flow Battery, Phd Thesis Dissertation Document, University of Iceland and the University of Akureyri, Reykjavík, Iceland, 2011.
[14] A.J. Bard, L.R. Faulkner, Electrochemical Methods. Fundamentals and Applications, Editorial Wiley, 2001.
[15] M.H. Chakrabarti, R.A. Dryfe, E.P. Roberts, Electrochim. Acta 52 (2007) 2189–2195.
[16] M. Li, T. Hikihara, Commun. Comput. Sci. E91A (2008) 1741.
[17] M. Moyabayashi, T. Tayama, Y. Kageyama, H. Oyama, U.S. Patent 5, 851,694, 1998.
[18] C. Bengoa, A. Montillet, P. Legentilhomme, J. Legrand, J. Appl. Electrochem. 27 (1997) 1313–1322.
[19] A. Wragg, A. Leontaritis, Chem. Eng. J. 66 (1997) 1–10.
[20] J. Collins, X. Li, D. Pletcher, R. Tangirala, D. Stratton-Campbell, F.C. Walsh, et al., J. Power Sources 195 (2010) 2975–2978.
[21] D.S. Aaron, Q. Liu, Z. Tang, G.M. Grim, A.B. Papandrew, A. Turhan, T.A. Zawodzinski, M.M. Mench, J. Power Sources 206 (2012) 450.
[22] C. Jia, J. Liu, C. Yan, J. Power Sources 195 (2010) 4380.
[23] J.Q. Cheng, B. Wang, J. Yang, Solvent Extr. Ion Exch. 27 (2009) 302.
[24] J.Q. Cheng, B. Wang, L. Hong-ling, Adv. Mater. Res. 236–238 (2011) 604–607.
[25] M. Lopez Atalaya, G. Codina, J.R. Perez, J.L. Vazquez, A. Aldaz, M.A. Climent, J. Power Sources 35 (1991) 225.
[26] L. Bin, L. Liyu, Wei Wang, Z. Nie, B. Chen, X. Wei, Q. Luo, Z. Yang, V. Sprenkle, J. Power Sources 229 (2013) 1–5.
[27] D.P. Scamman, G.W. Reade, E.P. Roberts, J. Power Sources 189 (2009) 1220–1230.
[28] T. Cebeci, P. Bradshaw, Momentum Transfer in Boundary Layers, McGraw-Hill, 1977.
[29] L.H. Norris, W.C. Reynolds, Turbulent Channel Flow with a Moving Wavy Boundary, Department of Mechanical Engineering, Stanford University, USA, 1975.
[30] M. Wolfstein, Int. J. Heat Mass Transfer 12 (1969) 301.
[31] W. Xu, Q. Chen, F.T.M. Nieuwstadt, Int. J. Heat Mass Transfer 41 (1998) 3161–3176.
[32] S. Al-Baghdadi, M.A.R. Al-Janabi, Eng. Appl. Comput. Fluid Mech. 1 (2007) 7–87.
[33] L. Yu, G. Ren, M. Qin, X. Jiang, Eng. Appl. Comput. Fluid Mech. 2 (2008) 344–353.
[34] J.B. Joshi, V.V. Ranade, Ind. Eng. Chem. Res. 42 (2003) 1115–1128.
[35] J.L.C. Santos, J.L.C. Geraldes, S. Velizarova, J.C. Crespo, Chem. Eng. J. 157 (2010) 379–392.
[36] S. David Moore, The Basic Practice of Statistics, third ed., W.H. Freeman and Company, New York, 2003.
[37] W. Navidi, Estadística para ingeniero y científicos, first ed., McGraw-Hill Companies, Inc., New York, 2006.